Ocean Modelling 121 (2018) 76–89

Contents lists available at ScienceDirect

Ocean Modelling

journal homepage: www.elsevier.com/locate/ocemod

Impact of increasing antarctic glacial freshwater release on regional sea-ice cover in the Southern Ocean

Nacho Merino[a], Nicolas C. Jourdain[*,a], Julien Le Sommer[a], Hugues Goosse[b], Pierre Mathiot[c], Gael Durand[a]

[a] Université Grenoble Alpes/CNRS/IRD/G-INP, IGE, Grenoble, France
[b] Universite Catholique de Louvain, Louvain-la-Neuve, Belgium
[c] Met Office, Exeter, UK

ARTICLE INFO

Keywords:
Southern ocean
Sea ice
Glacial freshwater

ABSTRACT

The sensitivity of Antarctic sea-ice to increasing glacial freshwater release into the Southern Ocean is studied in a series of 31-year ocean/sea-ice/iceberg model simulations. Glaciological estimates of ice-shelf melting and iceberg calving are used to better constrain the spatial distribution and magnitude of freshwater forcing around Antarctica. Two scenarios of glacial freshwater forcing have been designed to account for a decadal perturbation in glacial freshwater release to the Southern Ocean. For the first time, this perturbation explicitly takes into consideration the spatial distribution of changes in the volume of Antarctic ice shelves, which is found to be a key component of changes in freshwater release. In addition, glacial freshwater-induced changes in sea ice are compared to typical changes induced by the decadal evolution of atmospheric states. Our results show that, in general, the increase in glacial freshwater release increases Antarctic sea ice extent. But the response is opposite in some regions like the coastal Amundsen Sea, implying that distinct physical mechanisms are involved in the response. We also show that changes in freshwater forcing may induce large changes in sea-ice thickness, explaining about one half of the total change due to the combination of atmospheric and freshwater changes. The regional contrasts in our results suggest a need for improving the representation of freshwater sources and their evolution in climate models.

1. Introduction

The Southern Ocean plays a substantial role in the Earth system. For instance, it is a significant sink for the anthropogenic carbon dioxide (Sallée et al., 2012) and atmospheric heat (Roemmich et al., 2015), thus mitigating global warming. In addition, the Southern Ocean produces the Antarctic Bottom Water (AABW), which is distributed into the three main oceanic basins (Atlantic, Pacific and Indian). The AABW, a key driver of the global thermohaline circulation, ventilates the deep ocean due to its high oxygen content (Mantyla and Reid, 1983; Orsi et al., 1999). All these processes are directly impacted by the Antarctic sea-ice cover, its melting and its production.

Some studies have emphasized unexpected trends in Antarctic sea-ice cover over the last decades (e.g. Comiso, 2010). While the Arctic sea ice extent (SIE) presents a statistically significant decrease of 3.8% per decade, the Antarctic SIE presents a small but statistically significant increase of 1.2% per decade (Comiso et al., 2011). The net increase in Antarctic sea ice results from the combination of positive and negative regional trends. Even if the magnitude and the significance of the total increase remains open to debate (Polvani and Smith, 2013; Screen, 2011), the significance of regional trends in sea ice concentration (SIC) has a larger consensus in the community (Comiso et al., 2011). For instance, the Ross Sea SIE has increased by about a 5% per decade, while the SIE in the Amundsen-Bellingshausen Seas sector has decreased by up to 7% per decade (Turner et al., 2009). In addition, the trend in number of annual ice-covered days exhibits similar regional patterns: the Southern Ocean has gained up to 3–4 days per year of coverage in some locations of the Ross Sea, and has lost up to 3–4 days per year in sectors of the Bellingshausen Sea (Stammerjohn et al., 2012).

While the Artic SIE response to the climate change is strongly coupled with global atmospheric warming (Perovich, 2011), Antarctic sea ice trends seem to result from much more complex processes. It has been suggested that observed atmospheric trends in the Southern Annual Mode (SAM) index (Thompson et al., 2011) and the Amundsen Sea Low, which affect wind velocities, air temperature and humidity, may

* Corresponding author.
E-mail address: nicolas.jourdain@univ-grenoble-alpes.fr (N.C. Jourdain).

https://doi.org/10.1016/j.ocemod.2017.11.009
Received 13 June 2017; Received in revised form 28 November 2017; Accepted 30 November 2017
Available online 01 December 2017

partially explain the observed changes in the Antarctic sea-ice (Turner et al., 2009). The coupling between SAM and the El Nino Southern Oscillation (ENSO) may also contribute to the observed regional pattern of the trend (Stammerjohn et al., 2008; Kwok et al., 2016). However, the amplitude of the regional trends and the total increase in SIE does not seem to be completely explained by changes of atmospheric origin (Lefebvre and Goosse, 2008). In addition, other modeling studies have shown that an increased SAM trend produced by ozone depletion leads to sea ice reduction in climate models (Bitz and Polvani, 2012; Sigmond and Fyfe, 2010). This suggests that other mechanisms must be contributing to the observed trends in sea ice. Some of the non-atmospheric factors affecting the observed sea-ice distribution may be related to oceanic and sea-ice feedbacks. For instance, changes in the salt rejection associated with sea-ice changes and the freshening of the ocean surface may be affecting oceanic deep heat convection in some regions (Goosse and Zunz, 2014; Zhang, 2007).

The observed increase in mass loss from the Antarctic ice sheet (Rignot et al., 2011; Shepherd et al., 2012), may be contributing to salinity changes in the Southern Ocean (Jacobs et al., 2002; Jacobs and Giulivi, 2010). Enhanced continental ice discharge combined with the observed thinning of ice shelves (Pritchard et al., 2012; Paolo et al., 2015) has increased glacial freshwater injection into the ocean, at least since the beginning of the 1990s (Shepherd et al., 2012). This increase in glacial freshwater flux is usually not considered in climate models, which may explain why climate models have so far failed to predict trends and regional variability in SIE (e.g. Turner et al., 2013). Recent studies have investigated the response of Antarctic sea ice to the recent increase in glacial freshwater input to the ocean with a coupled model (Bintanja et al., 2013; Swart and Fyfe, 2013; Pauling et al., 2016). However, they differ in their main conclusions. In some cases, the impact of perturbations in the glacial freshwater forcing on sea ice is very weak and not significant. In other cases, the response is relevant but does not match the spatial pattern of the observations. This may be due to the lack of consensus over the quantity and spatial distribution of the freshwater perturbation applied in such experiments. Indeed, most ocean models present large differences in their freshwater forcing protocol and neglect the spatial distribution of the sources. Recent ice-shelf mass balance estimates based on satellite data (Rignot et al., 2013; Depoorter et al., 2013) may help better constrain both the magnitude and the spatial distribution of glacial freshwater released into the Southern Ocean. Furthermore, recent improvements in the methods to prescribe ice-shelf melt (Mathiot et al., 2017) and to distribute the iceberg meltwater through Lagrangian models (Merino et al., 2016; Marsh et al., 2015) now allow a better distribution of the Antarctic glacial freshwater over the Southern Ocean. This has been shown to affect sea ice production (Merino et al., 2016; Mathiot et al., 2017) but, as yet, it remains neglected by most ocean models.

In this study, we evaluate the impact of the recent enhancement in glacial freshwater fluxes on the sea ice properties in the Southern Ocean. Two different freshwater scenarios are proposed to represent the current and pre-imbalance ice-ocean mass fluxes. The scenarios are built upon glaciological estimates of the Antarctic ice mass loss, and distinguish calving from ice-shelf melt. Both glacial freshwater scenarios are applied to an atmospherically forced eddy-permitting ocean-sea-ice model. An improved version of a Lagrangian particle iceberg model is coupled with our ocean model in order to distribute the calved mass, while ice-shelf melt is prescribed following the method proposed by Mathiot et al. (2017). The sensitivity to changes in glacial freshwater scenario is addressed under the same atmospheric conditions then compared against typical changes induced by decadal atmospheric variability. Section 2 describes the model set-up and the freshwater forcing scenarios. Section 3 presents the model mean state and trends and Section 4 describes the model response to atmosphere and freshwater perturbations and discusses the related mechanisms.

2. Material and methods

2.1. Ocean/sea-ice model configuration

All the numerical experiments performed in this study share the same general model set up. Simulations use a coupled ocean/sea-ice/iceberg model with interannual atmospheric forcing. The ocean component is based on NEMOv3.5 (Madec, 2014) with a global grid of 0.25° resolution (ORCA025) developed by the DRAKKAR group. It considers 75 vertical z-levels with partial steps. The model is forced by atmospheric data from the interannual DFS5.2 re-analysis (ERA-Interim based, (Dussin et al., 2016; Brodeau et al., 2010)). It uses the CORE bulk formulations with three-hourly winds, humidity and air temperature, and daily cloud cover, short- and long-wave solar radiation and liquid and solid precipitations. The ocean component is coupled every time step with the LIM2 sea-ice model (Fichefet and Morales Maqueda, 1997). A salinity restoring term towards NODC WOA data (Gouretski and Koltermann, 2004) with a piston velocity of 50 m/300 days applied to the ocean surface (Griffies et al., 2009). This term is required in atmospherically forced simulations because of the missing atmospheric feedbacks (Griffies et al., 2009).

The ocean component is also coupled with the NEMO-ICB Lagrangian iceberg module (Marsh et al., 2015) containing the most recent improvements described in Merino et al. (2016). These latter modifications consider depth-dependent ocean velocities and temperatures in the computation of the drag and melt rate applied to icebergs, instead of ocean-surface properties as in most iceberg models so far. All the meltwater from icebergs is put at the ocean surface, i.e. assuming no significant mixing with the iceberg freshwater plume. Our model configuration does not include ice-shelf cavities, but adopts the parameterization developed by Mathiot et al. (2017) to distribute the observation-based ice-shelf meltwater from Antarctica. The later emulates the buoyancy-driven ice-shelf overturning by distributing the coastal runoff over the vertical model levels located between the depth of the ice-shelf front and the deepest depth of the glacier grounding line (or the bathymetry at the front if shallower than the grounding line). Mathiot et al. (2017) have shown that this method outperforms those in which the ice-shelf freshwater is injected at the depth of the ice-shelf front (e.g., Beckmann and Goosse, 2003). The prescribed amplitude of iceberg calving and ice-shelf melt is described in the next subsection.

Ocean temperature and salinity are initialized from the observational estimates from Steele et al. (2001), and Antarctic sea ice is initialized to 1 m thick wherever ocean surface is below −1 °C. All the experiments conducted in this study use a 11-year spin up phase, which is reasonable for initializing major circulation features and surface properties (Barnier et al., 2006; Tréguier et al., 2010), and to balance the iceberg mass and melt water from the iceberg module (Merino et al., 2016). After the 11-year spin up, the drift in ACC transport at Drake is 0.2 Sv/yr, exactly as in Tréguier et al. (2010) who used a very similar NEMO configuration and attributed the drift to an erosion of AABW along the simulations. It is therefore likely that dense water formation and/or its downward transport are poorly represented in our model. Nonetheless, no significant drift of surface fluxes is found after the spin up phase (not shown), and our methodology prevents our results from being affected by any potential drift because we mostly compare experiments of similar drifts (see Section 2.3).

2.2. Freshwater forcing in the southern ocean

This section explains how our freshwater forcing is constructed and how our experiments are designed to address the main question of this study. In the Southern Ocean, the glacial freshwater fluxes come from melting icebergs and ice-shelves (the floating extension of outlet glaciers confined in an embayment). In the following, we present the terms of the ice-shelf mass balance (Section 2.2.1), the recent observational estimates of calving flux and ice-shelf melt used to build our mean

freshwater forcing over the 2000–2009 period (Section 2.2.2), and (the method developed to reconstruct the mean calving flux and ice-shelf melt over the 1990–1999 period (Section 2.2.3).

In the Southern Ocean, glacial freshwater fluxes come from the melting of ice originating from the Antarctic Ice Sheet. As we will see in Section 2.2.1 and as already conceptually introduced by Rye et al. (2014) and Pauling et al. (2016), the amount of glacial freshwater getting into the ocean is strongly affected by changes in the mass of ice shelves. The glacial freshwater fluxes can be estimated for the major ice shelves over the 2000–2009 period based on observational studies and accounting for the changing mass of ice shelves (Section 2.2.2). A number of hypotheses then allow constraining a glacial freshwater scenario representative of the 1990s, as described in Section 2.2.3. To date, no reliable information can be considered for the reconstruction of time-varying glacial freshwater fluxes between the two periods, so we will run sensitivity experiments in which we apply the two freshwater fluxes, with constant fluxes over the entire simulations (see Section 2.3). Such experimental design is similar to Bintanja et al. (2013, 2015) and Pauling et al. (2016). The analysis of the mean anomalies provides information on the impact of freshwater on the Antarctic sea ice. Prescribing a ramping versus constant freshwater flux may affect the estimation of sea ice trends within a simulation, but comparing the mean sea ice between two simulations with constant freshwater forcing does not require any assumption on the ramping shape.

2.2.1. The ice shelf mass balance equation

The freshwater flux into the Southern Ocean can come from three continental sources: icebergs melting along their trajectories, basal melt underneath ice shelves, and runoff from surface melting. The later is mostly confined to a few regions in the Northern Antarctic Peninsula (Barrand et al., 2013; van den Broeke, 2005), although it can sporadically be observed in other regions (e.g. Nicolas et al., 2017; Bell et al., 2017). Furthermore, most of the surface melt water refreezes before reaching the ocean (Irvine-Fynn et al., 2011). Therefore, the freshwater flux from surface melting is usually neglected compared to the freshwater flux associated with the calving flux (CF) and the ice-shelf basal mass balance (BMB).

To understand these two prominent freshwater fluxes, one needs to consider the mass balance of an ice shelf. A schematic view of an Antarctic ice shelf is shown in Fig. 1, which describes the main mass fluxes, ocean currents, and other terms that are used throughout this paper. Antarctic ice shelves gain mass from the ice inflow through the grounding line gate (imaginary surface between the floating and grounded ice) and due to snowfall at their surface. Their mass loss occurs through several processes: calving at their front, basal melt at the ocean-ice interface, and wind erosion or sublimation at their surface.

From the ice shelf point of view, the two fluxes of interest for the ocean, i.e. CF and BMB, are partly compensated by the surface mass balance (SMB) (which includes snow accumulation, surface melting/refreezing, sublimation, snow erosion and transport by the wind) and the grounding line flux (GLF). The difference between the inputs (GLF, SMB) and outputs (CF, BMB) results in the mean thickening rate (dh/dt) or ice shelf mass convergence. The mass conservation is thus described by the following equation (Rignot et al., 2013; Depoorter et al., 2013):

$$dh/dt = \mathrm{SMB} + \mathrm{GLF} - \mathrm{CF} - \mathrm{BMB} \quad (1)$$

In the following paragraphs, we describe the two different glacial freshwater scenarios applied to our ocean simulations. Basically, our approach consists of determining a pair of CF and BMB values for: (i) a scenario corresponding to the mass exchange between the Antarctic ice shelves and the ocean in the 2000s (*FRESH+*) and (ii) a scenario representative of the situation in the early 1990s (*FRESH−*). This latter scenario, built from *FRESH+*, is based on assumptions on the various terms of the ice shelf mass balance (Eq. (1)) and computed for each ice shelf larger than 100 km^2. Details on the construction of both scenarios, *FRESH+* and *FRESH−*, are given in Sections 2.2.2 and 2.2.3 respectively, and a summary of the two glacial freshwater scenarios with all the terms of Eq. (1) is presented in Fig. 2. A detailed comparison of the BMBs corresponding to the two glacial freshwater scenario is shown in Fig. 3 for each individual ice shelf.

2.2.2. Scenario FRESH+

Scenario *FRESH+* represents the Antarctica/Southern Ocean freshwater exchanges of the decade 2000–2009. We therefore directly use the CF and BMB fluxes provided by Depoorter et al. (2013). These estimates are based on data from the ICESat period (2003–2009) and

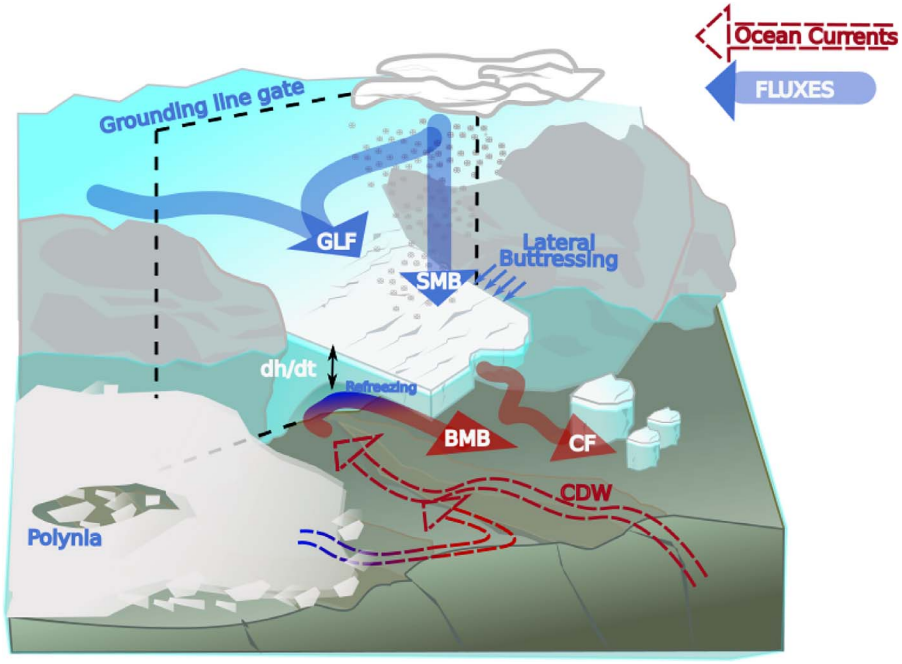

Fig. 1. Schematic diagram of idealized Antarctic ice shelf, showing some ocean currents (dashed) and the fluxes involved in the ice-shelf mass balance: Grounding Line Flux (GLF), Surface Mass Balance (SMB), Calving Flux (CF), Basal Mass Balance (BMB). CDW stands for Circumpolar Deep Water.

	dh/dt	= SMB	+ GLF	- CF	- BMB
FRESH+	-282	444	2049	1321	1454
	Ice shelves balanced	Preserved	Corrected with Shepherd 2012	Preserved	Estimated in this work
FRESH-	0	444	1978	1321	1101

Fig. 2. *FRESH+* and *FRESH−* full Antarctica integrated terms of the ice-shelf mass balance (Eq. (1)). Red numbers correspond to the terms having been modified in the *FRESH−* scenario with respect to the *FRESH+* scenario. Black numbers correspond to quantities that remain the same in both scenarios. Units are Gt/yr.

previous satellite programs (including ERS-1 and ERS-2) covering a large part of the 1990–1999 decade in many regions. The scenario accounts for ice-shelf thinning rates that are consistent with the observed enhancement of Antarctic mass discharge. In Depoorter et al. (2013), all the sparse collected data were corrected in time to get estimates representative of the decade 2000–2009. This means that their estimates provide a reasonable representation of the annual glacial freshwater fluxes that were released into the Southern Ocean over that decade, and are consistent with other recent estimates over the same period (Rignot et al., 2013).

All the ice shelf locations considered in Depoorter et al. (2013) have been identified on our ORCA025 model grid following Merino et al. (2016). For a given ice shelf, the BMB flux is homogeneously distributed over all grid points along the corresponding ice shelf front, and distributed vertically according to the ice-shelf geometry, as described in Section 2.1. In addition, Depoorter et al. (2013) provide an upscaling mass flux term per oceanic basin so that the total estimated Antarctic mass loss can be matched. The latter is homogeneously distributed over the coastal surface grid points of the corresponding oceanic basin. Our forcing strategy does not consider any seasonal variations in BMB, because very little is known about such seasonality. The CF estimates are used as inputs for the Lagrangian iceberg model. CF values are kept constant over time with the same calving rates and locations as provided in Merino et al. (2016). The ocean/iceberg model distributes the iceberg meltwater over the Southern Ocean, with seasonal variations related to the ocean properties (Merino et al., 2016).

2.2.3. Scenario FRESH−

The *FRESH−* scenario is designed to represent a reasonable glacial freshwater input into the ocean before the observed Antarctic mass imbalance, in the early 1990s (Rignot et al., 2011; Shepherd et al., 2012). The recent acceleration of grounded outlet glaciers is linked to the thinning of ice shelves as a consequence of the enhancement of their basal melting (Pritchard et al., 2012) or collapse (Scambos et al., 2004). Our hypothesis is that the Antarctic ice shelves were in steady state in the early 1990s ($dh/dt = 0$). This assumption may not be entirely true at the regional scale, as it is known that some glaciers in the Amundsen sector were already retreating early in the 80s (Hughes, 1981; Smith et al., 2016), and the Ross Sea was already experiencing freshening in the early 1990s (Jacobs and Giulivi, 2010). It is nonetheless a good approximation at the scale of Antarctica (Paolo et al., 2015), and making other assumptions regionally is not straightforward. This assumption may nonetheless result in an overestimation of the glacial freshwater differences between the scenario *FRESH+* and *FRESH−* in the Amundsen sector.

To construct the *FRESH−* scenario, we start from the estimates provided by Depoorter et al. (2013). In addition to setting dh/dt to zero, further hypotheses regarding SMB, CF and GLF are needed to compute BMB from Eq. (1). The SMB values in Depoorter et al. (2013) are from a regional atmospheric simulation over 1979–2010, assuming that there has been no significant SMB trend over that period (Monaghan et al., 2006; Lenaerts et al., 2012). We therefore keep the same SMB values as in Depoorter et al. (2013), as they are also representative of the 1990s. We make a similar assumption for the CF term because, to our knowledge, there is no evidence of any trend in calving fluxes. Of course, individual events of ice shelf collapse may introduce interannual variability in CF (Rott et al., 1996), but it would be difficult to associate a statistically significant trend to these events (Liu et al., 2015). It has to be noted that some observed changes in ice-shelf velocities are compensated by changes in ice shelf thickness, so that the ice mass flow is relatively unchanged, which is consistent with the small changes in the position of calving fronts observed over the recent decades.

Now we estimate GLF in the early 1990s so that we can deduce BMB from Eq. (1). To do so, we use estimates of Antarctic contributions to sea-level rise (i.e. of mass loss of the grounded ice sheet) since the beginning of the 1990s. The mass equation for the grounded part is:

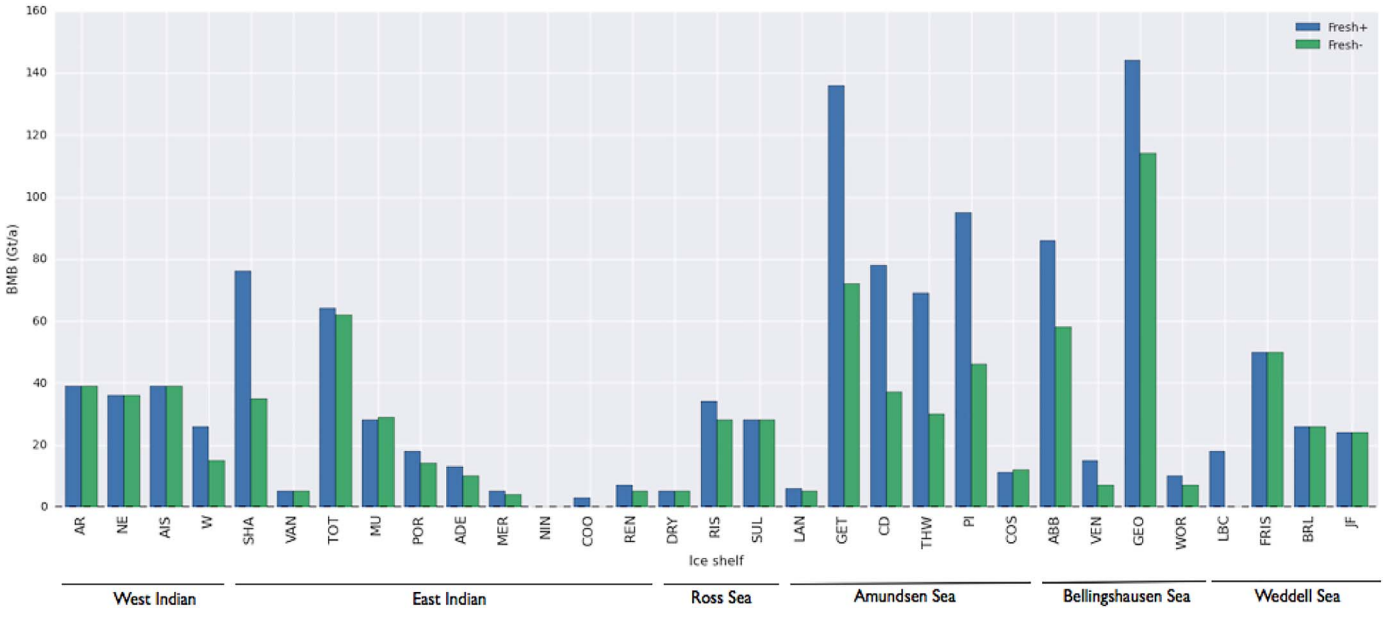

Fig. 3. Basal Mass Balance (BMB) per ice shelf (Gt/yr) considered in the *FRESH+* (blue bars) and *FRESH−* (green bars) glacial freshwater scenarios. Ice shelf names and the oceanic sectors are based on the definitions of Depoorter et al. (2013). (For interpretation of the references to color in this figure legend, the reader is referred to the web version of this article.)

$$\frac{dM}{dt} = \mathrm{SMB_{gr}} - \mathrm{GLF} \tag{2}$$

where M is the mass of grounded ice, GLF the grounded line flux, and $\mathrm{SMB_{gr}}$ the surface mass balance of the grounded part of glaciers.

For some glaciers in West Antarctica, in the Antarctic Peninsula (like Larsen ice shelves), and in the East Indian sector of East Antarctica (Totten and Cook), the grounded ice mass loss has been explained by changes in ice dynamics (Rignot et al., 2008; 2002). For these glaciers, we can therefore express GLF in the early 1990s as:

$$\mathrm{GLF_{1990s}} = \mathrm{GLF_{2000s}} + \left(\frac{dM}{dt}\right)_{1990s} - \left(\frac{dM}{dt}\right)_{2000s} \tag{3}$$

where each quantity is an average over the period in subscript. We now assume that the ice sheet was approximately in steady state in the early 1990s, so that the second term in the right hand side of Eq. (3) is neglected. We then assume that the third term in the right hand side of Eq. (3) is given by the observational estimates of Shepherd et al. (2012). As $\mathrm{GLF_{2000s}}$ is known from Depoorter et al. (2013), we can deduce $\mathrm{GLF_{1990s}}$. For the other glaciers, no dynamical changes have been reported, and mass changes between the 1990s and the 2000s have been attributed to regional changes in surface mass balance ($\mathrm{SMB_{gr}}$). In these cases, it is reasonable to assume that GLF has remained unchanged between the 1990s and the 2000s.

Our backward estimation of GLF is based on two major assumptions. First, we assume that Antarctica was in steady state in the early 1990s. The validity of this assumption is uncertain, for example, Shepherd et al. (2012) suggest that the Antarctic ice sheet was gaining mass in the early 1990s, which would mean that the perturbation introduced between *FRESH+* and *FRESH−* is globally underestimated, although the rate of mass change in the early 1990s is likely negligible compared to the perturbation we introduce. Second, we assume that the rates of mass change provided by Shepherd et al. (2012) are representative of the 2000s, while they actually represent the period 1992–2011. This may again imply an underestimation of the GLF differences between the *FRESH+* and *FRESH−* scenarios since many drainage basins have experienced a strong mass loss acceleration over the recent decades, particularly in the Amundsen sector (Rignot et al., 2011; Sutterley et al., 2014)

Our methodology to construct freshwater scenarios is new in the sense that previous studies analyzing the impact of glacial freshwater perturbations on the Southern Ocean sea-ice were based on empirical perturbations (Pauling et al., 2016) or on sea-level rise estimates (Bintanja et al., 2013; Swart and Fyfe, 2013). As pointed out by Rye et al. (2014), these commonly used approaches neglect ice shelf thinning or thickening, and do not make any difference between mass changes of dynamical origin and those originating from changes in the surface mass balance. The ice shelves are the Antarctic glacial freshwater exchangers with the ocean, and therefore, the construction of glacial freshwater scenarios should always consider the ice shelves processes and their mass balance equation.

2.3. Model experiments

Three model experiments are performed to study the sensitivity of the model to different forcing perturbations (Fig. 4). The three runs use the model set-up described in Section 2.1 and cover 31 years, including 11 years of spin up that are not analyzed in the following. The three experiments consider a constant glacial freshwater forcing over the full experiment period because the timing of the changes in freshwater fluxes is poorly known. In terms of timing of the freshwater release, our experimental design is thus similar to Bintanja et al. (2013, 2015) and Pauling et al. (2016). Swart and Fyfe (2013) and Pauling et al. (2017) used a different method, considering melt rates that vary linearly in time. However, observational studies suggest that mass changes have occurred at an accelerated rather than constant rate, with distinctive

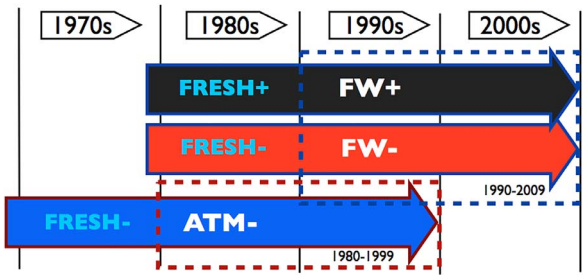

Fig. 4. Schematic diagram showing the experiments conducted in this study. FW+ considers the *FRESH+* glacial freshwater scenario and was run for a 31-year period starting in 1979. FW− uses the *FRESH−* scenario and covers the same time period as FW+. ATM− uses the *FRESH−* scenario and was run for a 31-year period starting in 1969.

regional patterns of acceleration (Rignot et al., 2011; Sutterley et al., 2014), so we have preferred not to make any assumption on the freshwater trend. Prescribing a ramping versus constant freshwater flux may affect the estimation of sea ice trends within a simulation (Pauling et al., 2017), but here we compare the mean sea ice cover between two simulations with constant freshwater forcing rather than directly comparing the trends. Our methodology therefore does not rely on any assumption on the detailed timing of the freshwater release, and the difference between the two simulations with different freshwater scenarios does represent the typical increase in freshwater release over the recent decades. We further note that comparing perturbed mean states rather than trends is also a way to remove the influence of model drifts.

The control run, hereafter the FW+ experiment simulates the period 1979–2009 with the freshwater scenario *FRESH+* described in Section 2.2.2. The FW− simulation considers the same period (1979–2009) as the FW+ run, but with the freshwater scenario *FRESH−*. Finally, the ATM− run combines the application of the perturbed scenario *FRESH−* and an atmospheric forcing period starting and finishing 10 years earlier than the other runs, thus covering the period 1969–1999. This 10-year lag in the atmospheric forcing is equivalent to the approximative 10-year lag in the freshwater perturbation (FW+ minus FW−). It should be noted that 10 of the 11 years of spin up in the ATM− experiment use atmospheric forcing before the satellite era (DFS5, based on the ERA-40 reanalysis prior to 1979). However, all our results are computed after the spin up period, i.e. when the atmospheric forcing is constrained by satellite data. Importantly, the impact of the different spin up between ATM− and the rest of experiments over 1990–1999 is small compared to the sensitivity reported in this paper (not shown). Fig. 5 shows the mean atmospheric perturbations introduced between the FW− and ATM− simulations. DFS5.2 tends to be dryer over the recent decades, with two exceptions in the region between the Ross and Amundsen Seas, and in the western Weddell Sea. Over the recent decades, air temperature tends to be warmer in the Amundsen and Bellingshaussen Seas, the Indian sector, and the northern Weddell Sea, but it tends to be markedly colder (by up to −1.5 °C) north of the Ross Sea and in the coastal Weddell Sea and West Pacific sector. Winds are stronger in the Atlantic and West Indian sectors and in some coastal regions of the Ross and Pacific sectors, and weaker from the Western coast of the Peninsula to the Amundsen Sea.

A schematic diagram of the three experiments is shown in Fig. 4. The comparison between FW+ and FW− provides an estimate of the model response to our perturbation in glacial freshwater forcing. Although there remain large uncertainties, this perturbation is a reasonable estimate of the typical decadal change in the freshwater released by the Antarctic continent into the ocean. In the results and discussion sections, the FW+ minus FW− comparison will therefore be referred to as *freshwater-induced* changes. The FW− versus ATM− comparison provides an estimate of the impact of the recent decadal atmospheric changes present in the ERA-Interim reanalysis. This comparison will

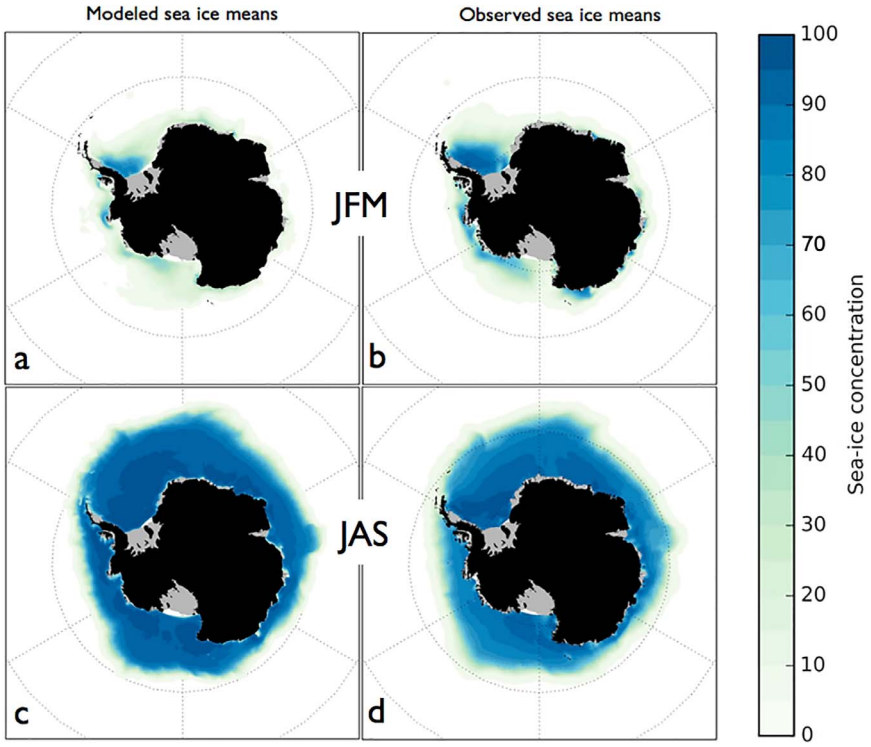

Fig. 5. Atmospheric anomalies in DFS5.2 reanalysis for: a) surface humidity, b) surface air temperature, and c) surface wind velocity. Anomalies are calculated as the 20-year average over 1990–2009 minus the 20-year average over 1980–1999.

therefore be referred to as *atmospheric-induced* changes. Finally, the FW + minus ATM − comparison accounts for both the perturbation in the glacial freshwater flux and in the decadal atmospheric forcing. This comparison indicates the typical decadal change in the Southern Ocean, as *FRESH* + represents the 2000s and *FRESH* − the early 1990s. Hereafter, it will be referred to as *total* changes.

3. Evaluation of the simulations

This section evaluates the ability of the model to represent the ocean and sea ice mean states, and sea ice variability. The simulated climatological sea-ice concentration (SIC) is compared to the NSIDC SIC in Fig. 6. Overall, the model set-up is able to reproduce the main spatial distribution with a SIC of similar magnitude as in the observations in both summer and winter. The model nonetheless has a deficit of sea ice in summer, with less concentrated sea ice in the West Pacific and the Amundsen sectors and a smaller extent of permanent sea-ice in the Weddell Sea than in the observations. This summer deficit is typical of ORCA025 simulations, and was also found in most ocean/sea-ice models forced by another atmospheric reanalysis (Downes et al., 2015). The model also produces too much sea ice over the winter months, exhibiting a more concentrated ice pack at the sea ice margins, as in other NEMO simulations presented in Downes et al. (2015). The reason for such biases is still a matter of research.

Fig. 7-a and b show the sea-ice trends computed from experiments FW + and FW − respectively. Both simulations present a very similar trend in SIC because they are forced by the same atmosphere. The simulations reproduce reasonably well the main observed patterns in SIC trends (Fig. 7-c), i.e. the positive trend offshore of Dronning Maud Land and in the Northern Ross Sea are well reproduced, as well as the negative trends on the Western flank of the Peninsula. Nonetheless, the model does not reproduce the observed sea ice trends along the ice sheet margins in the Pacific sector and in Prydz Bay. It should be noted that Holland et al. (2014) also managed to reasonably reproduce the observed trends in atmospherically forced ocean hindcasts, with regional biases of similar magnitude as in our study.

For the reasons mentioned in Section 2.3, we apply constant rather than ramping freshwater fluxes. Therefore, the effect of different freshwater fluxes between the early 1990s and the 2000s is not seen in the trend of individual simulations, but rather in comparisons of simulations with different freshwater fluxes. The *total* decadal SIC change (FW + over 1990–2009 vs ATM − over 1980–1999) is therefore compared to observations (1990–2009 vs 1980–1999) in Fig. 8. It should be noted that this decadal difference gives slightly different results compared to linear trends, in particular in the Weddel and Amundsen Seas (Fig. 7-c vs Fig. 8-b). Again, the main patterns of the *total* decadal SIC change are reasonably well reproduced by our simulations (Fig. 8). There are nonetheless significant differences offshore in the Amundsen and Bellingshausen Seas. By contrast to the offshore sea ice pack, the trends in these regions are well reproduced near the ice sheet margins. Further investigations indicate that the offshore bias is particularly affected by differences in the spin up between the ATM − and FW + experiments, and the positive offshore trend is actually attributed to a spurious signal inherited from the spin up (not shown). These offshore trends are therefore not analyzed in the following.

Finally, we have also made other comparisons to observational estimates that we briefly mention here. The patterns and amplitude of the simulated eddy kinetic energy (EKE) was found to be in good agreement with the EKE derived from AVISO (see Fig. 2 in Dinniman et al., 2015; not shown). The simulated barotropic transport through the Drake Passage remains within the observed range of 134 ± 11 Sv (Cunningham et al., 2003) all along the simulation, despite the drift of 0.2 Sv/yr mentioned in Section 2.1 (not shown).

4. Role of the atmospheric and freshwater perturbations on the sea ice decadal changes

To analyse and discuss our results, we define three regional sectors of analysis in the Ross Sea, the coastal Amundsen Sea, and West Pacific/East Indian sector (see Fig. 8-a). These sectors are chosen because they are significantly affected by changes in freshwater fluxes, because they are better able to reproduce the observational SIC changes than other locations, and because each of these boxes is affected by changes in freshwater fluxes through a specific mechanism.

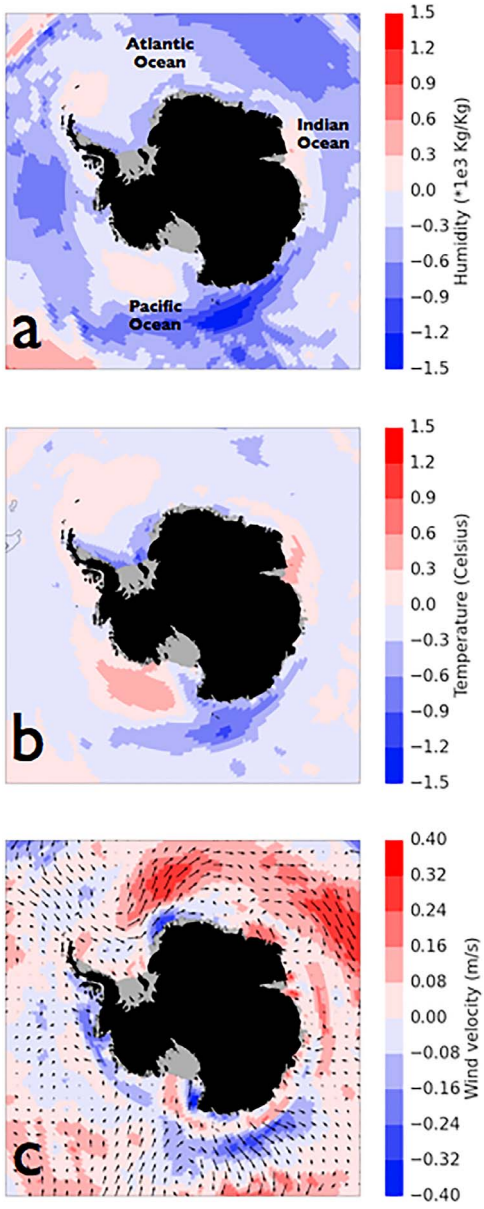

Fig. 6. Climatological sea-ice concentration (SIC) for: a) summer model results, b) summer observations, c) winter model results, d) winter observations. Summer months correspond to January, February and March and winter months to July, August and September. The model climatologies are calculated as the average over the last 20 years of simulations FW+ and ATM−. The observations climatology is calculated from NSDIC sea-ice concentration over the period 1979–2009.

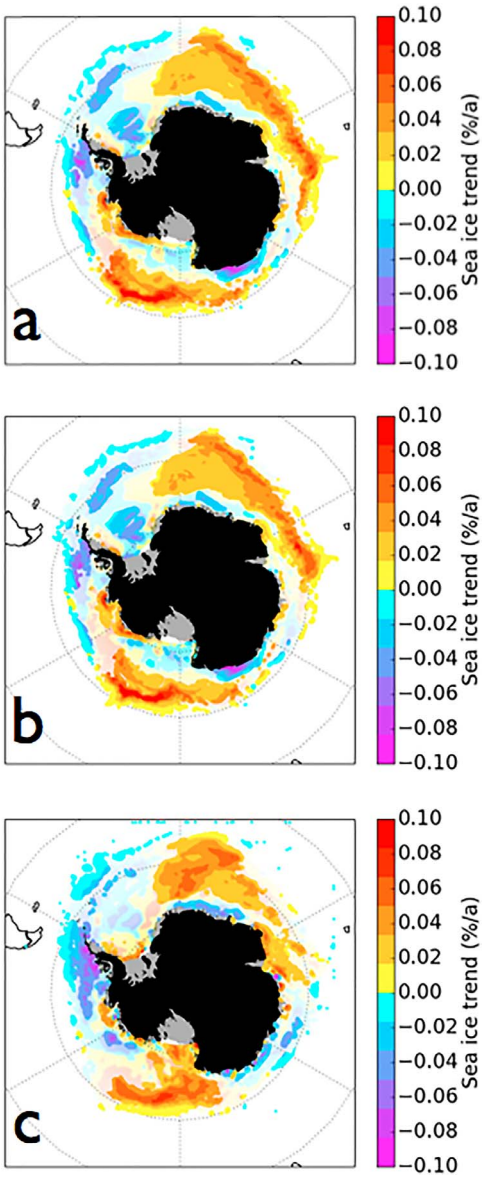

Fig. 7. Linear regression of the evolution of sea-ice concentration in: a) the FW+ experiment over 1990–2009, b) the FW− experiment over 1990–2009, and c) NSDIC observations over 1990–2009. Bright to faint shade indicates the level of significance, with faint colors indicating non-significant trends (determined by two-sided test for $p < 0.05$).

4.1. Mean sea-ice response over the whole Southern Ocean

Here we simply describe the general sea-ice response to the atmospheric and freshwater perturbations. The specific response of individual sectors and the corresponding mechanisms are described in the next sub-sections.

Qualitatively, the *total* modeled changes in SIC (due to both atmosphere and freshwater changes) are globally dominated by the atmospheric perturbation, especially in the Atlantic and West Indian sectors where the freshwater perturbation barely affects the SIC (Fig. 9). There are nonetheless other sectors where the freshwater perturbation significantly contributes to the *total* changes, such as in the Ross, Amundsen Sea, and West Pacific sectors. The quantitative comparison between FW+ and ATM− indicates a *total* change in sea ice extent (SIE) of about 3.0% for the whole Southern Ocean, and the *freshwater-induced* change accounts for about 25% of this *total* change (calculated as the ratio between the *freshwater-induced* signal and the *total* signal). The *freshwater-induced* changes in sea-ice thickness (SIT) are relatively more important than the corresponding changes in SIC. The SIT response is again negligible in the Atlantic and West Indian sectors, but is relatively strong in the other sectors (Fig. 10). The *total* annual change in integrated sea-ice volume (SIV) over the whole Southern Ocean is an increase of 2.8%, of which 46% is induced by the perturbation in glacial freshwater fluxes.

In terms of seasonality, the SIE response is dominated by the atmospheric changes during the ice-covered months, i.e. from March to October, while it is dominated by the freshwater changes during the melting months, i.e. from December to February (Fig. 11-a). The seasonal response of SIV is similar in timing, but the relative difference between the *atmosphere-induced* and the *freshwater-induced* parts is smaller than for the SIC (Fig. 11-b). The timing of sea ice minima and maxima (Table 1) and (the Ice Season Duration (ISD, as defined in Stammerjohn et al., 2008) are much more affected by the atmospheric perturbation than by the freshwater perturbation. The *total* ISD change

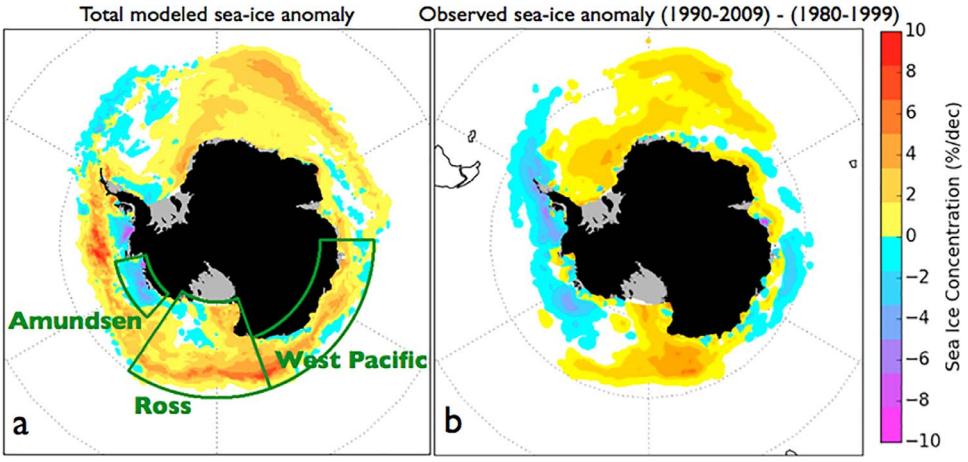

Fig. 8. Sea-ice concentration changes in percentage for: a) experiment FW+ over 1990–2009 minus ATM− over 1980–1999, and b) NSIDC observations over the period 1990–2009 minus 1980–1999.

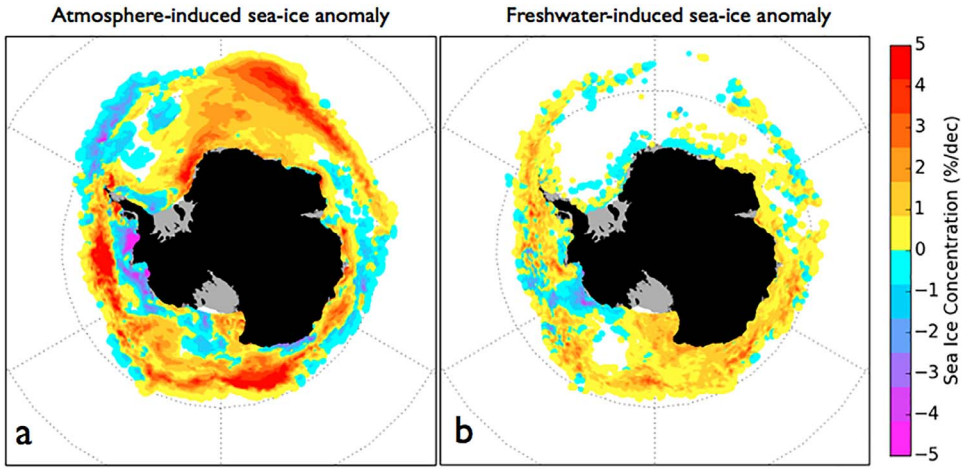

Fig. 9. Sea-ice concentration changes in percentage for: a) experiment FW− minus ATM−, and b) experiment FW+ minus FW−. Model means are annual averages over the last 20 years of the considered experiments.

(Fig. 12) is in good agreement with the ISD trend observed over 19792011 (Stammerjohn et al., 2012), even though the magnitude of the observed trend is slightly larger than in our simulations. This may be related to the fact that our model experiments (ocean-forced simulations) do not account for coupled processes between the ocean surface and the atmosphere, which would arguably amplify the impact of the *freshwater-induced* changes on sea ice (because the signal would not be damped by surface salinity restoring).

4.2. Sea-ice response in the West Pacific/East Indian sector

In the West Pacific/East Indian sector, the SIE increases by 5% in response to the *total* perturbation, and 52% of this increase is induced by the freshwater perturbation. The SIV increases by 10% in response to the *total* perturbation, and 61% of this increase is induced by the freshwater perturbation. Regarding the seasonality, both the freshwater and atmospheric perturbations contribute to increase the sea ice extent and volume over most of the year. The relative importance of the two perturbations varies between SIE and SIV, but the freshwater perturbation has a stronger relative importance in late summer and spring (from August to November). While the freshwater has only a weak influence on the phase of the seasonal cycle, the atmosphere perturbation advances the maximum by 10 days, delays the minimum by 3 days on average (Table 1), and (increases the SID (Fig. 12).

The *atmosphere-induced* sea ice changes in this sector were already described by Holland and Kwok (2012) and Holland et al. (2014) in terms of wind-driven thermodynamical changes. We therefore focus more on the mechanisms explaining the *freshwater-induced* changes. The freshening of the ocean surface may increase density differences between ocean surface and sub-surface water masses. This leads to a reinforcement of the density stratification between the ocean surface and subsurface (separated by the pycnocline), affecting the convection regime and therefore the heat supply from the deeper and warmer ocean to the ocean surface. This process, suggested by Marsland and Wolff (2001), may affect thermodynamical sea ice formation, resulting in more sea ice in presence of ocean surface freshening. A comparison of Fig. 13-a and b indeed suggests that the *freshwater-induced* increase in sea ice production along the coast is mostly explained by changes in oceanic heat flux at the sea ice base. This extra sea ice produced along the coast is then advected offshore, explaining the positive *freshwater-induced* sea ice anomaly all over this sector (Fig. 9b).

4.3. Sea-ice response in the Ross Sea

In the Ross sector, the SIE increases by 1.4% in response to the *total* perturbation, and 35% of this increase is induced by the freshwater perturbation. As much as 80% of the *total* increase in SIV is induced by the freshwater perturbation. Regarding the seasonality, the *freshwater-induced* thickening compensates for the *atmosphere-induced* thinning in summer (December and January). In spring and early summer, both the atmosphere and freshwater perturbations tend to favor the sea ice extension and thickening, with a dominant impact of the atmosphere on the SIE, but impacts of comparable magnitude for the SIV. While the freshwater has only a weak influence on the phase of the seasonal cycle, the atmosphere perturbation advances the maximum by 15 days on average (Table 1) and (increases the SID (Fig. 12).

As in the West Pacific/East Indian sector, the *atmosphere-induced* sea ice changes in the Ross Sea were already described by Holland and

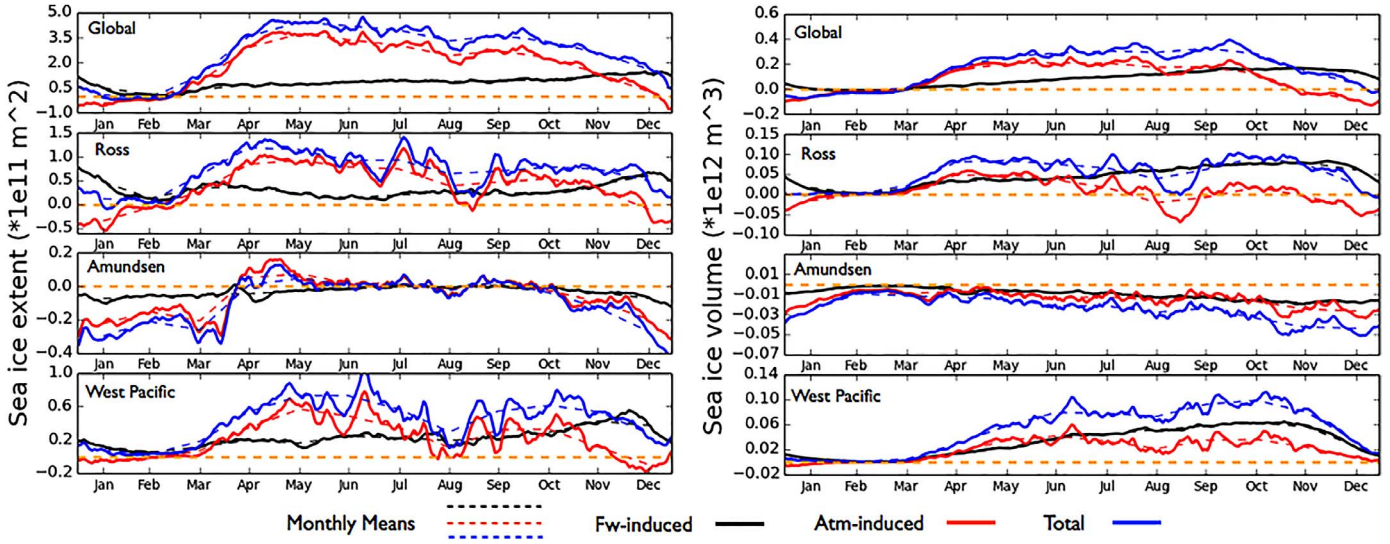

Fig. 10. Sea-ice thickness changes (in meters) for: a) FW− minus ATM−, and b) FW+ minus FW−. Averages are calculated over the last 20 years of the simulations.

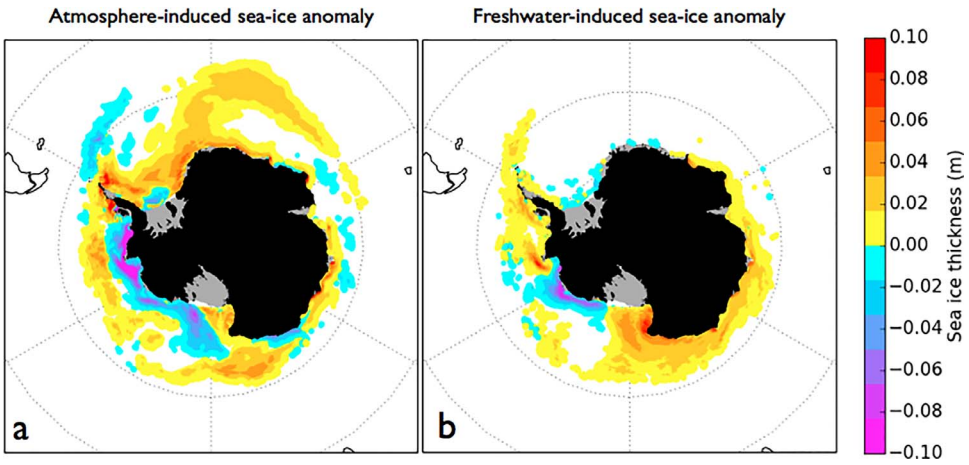

Fig. 11. Time series of anomalies of: a) sea-ice extent, and b) sea-ice volume, integrated over the whole Southern Ocean or regionally over the Ross, Amundsen and West Pacific sectors. The *freshwater-induced* changes (solid black) are obtained from FW + minus FW−, the *atmosphere-induced* changes (solid red) from FW− minus ATM−, and the *total* changes (solid blue) from FW+ minus ATM−. Dashed lines correspond to monthly averages and the orange dashed line provides the 0 reference. (For interpretation of the references to color in this figure legend, the reader is referred to the web version of this article.)

Table 1
Regional and total annual sea ice volume maxima and minima for the FW+, FW− and ATM− simulations, with the corresponding day of the year when these maxima and minima occur on average.

Region	Run	Maximum		Minimum	
		Day	SIV ($\times 10^{11}$ m^3)	Day	SIV ($\times 10^{11}$ m^3)
Global	FW+	264	147.5	49	2.97
	FW−	263	146.1	49	3.00
	ATM−	261	143.2	49	2.99
Ross	FW+	258	26.2	45	0.29
	FW−	258	25.9	44	0.26
	ATM−	243	25.8	44	0.26
Amundsen	FW+	216	5.55	53	0.16
	FW−	216	5.53	47	0.18
	ATM−	220	5.59	56	0.22
West Pacific	FW+	247	12.9	56	0.12
	FW−	247	12.7	56	0.12
	ATM−	237	12.4	59	0.12

Kwok (2012) and Holland et al. (2014) in terms of wind-driven thermodynamical changes, and here we focus on the mechanisms explaining the *freshwater-induced* changes. A similar mechanism as in the West Pacific/East Indian sector can explain the sea ice response to the freshwater perturbation. As shown in Fig. 13-b, the Ross Sea presents an increase in thermodynamical sea-ice production at the coast where the ocean surface is much fresher (Fig. 14 b). The freshwater perturbation results in a SIV increase of 8.1 $\times 10^{10}$ m^3 during the sea-ice production months (from March to September). The extra SIV produced in the FW + simulation (compared with the FW− simulation) is found mostly along the coast and is advected, resulting in increased SIC (Fig. 8) and (SIT (Fig. 10). This northward export of sea-ice in the Ross sector is further supported by a strengthened Antarctic Coastal Current (ACoC), which is visible in Fig. 14-a as a *freshwater-induced* rise in sea surface height, in good agreement with Rye et al. (2014). The stronger ACoC contributes to the *freshwater-induced* changes in sea-ice divergence in this sector. These changes represent a mean SIV loss of 1.7 $\times 10^{10}$ m^3 per year, which is relatively weak compared with the changes of thermodynamical origin in this sector.

As shown in Table 1, the SIV differences in minima between the FW + and FW− simulations are not significant compared with the SIV differences in maxima. Given the extra SIV produced by FW+, there is an excess of sea ice that needs to be melted during the spring and summer months if both simulations are to show relatively similar sea-ice minima. According to Table 1, the sea-ice minimum obtained in the sector does not seem to be much affected by the freshwater or atmospheric perturbations introduced in our experiments. However, in the FW+ simulation, the melting of sea-ice is amplified by summer *freshwater-induced* changes in the oceanic heat reaching the sea-ice base (see Fig. 15-a). In contrast to the annual means (Fig. 13-a), the oceanic heat supplied to the sea-ice base in summer is slightly greater in the FW+

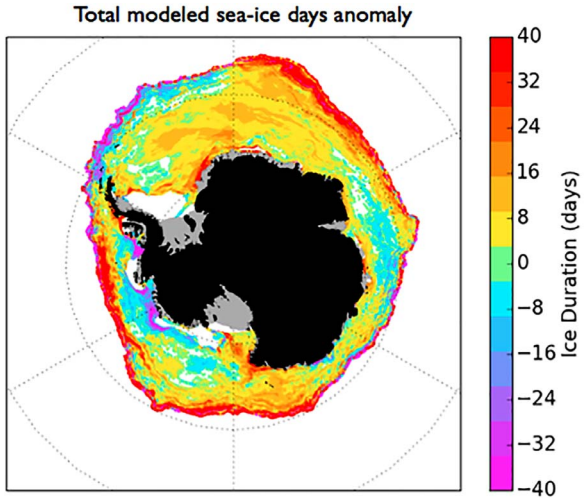

Fig. 12. *Total* changes (FW+ minus ATM−) in Ice Season Duration as defined by Stammerjohn et al. (2008).

simulation than in the FW− simulation (represented by lower heat in sea-ice formation equivalent in Fig. 15-a). This may be related to a sea-ice feedback, which helps compensate for the extra sea-ice volume produced in winter. When the sea-ice retreats in late spring, the thicker sea-ice produced in FW+ results in colder summer SST (as shown in Fig. 15-b). The colder and denser sea surface affects buoyancy and therefore reduces the density stratification. Under these specific conditions, the oceanic heat convection in summer is facilitated in the sector as shown in Fig. 15-a. However, this extra oceanic heat is not able to entirely explain the extra sea-ice melting in the Ross sector obtained in the FW+ simulation.

4.4. Sea-ice response in the coastal Amundsen Sea

The sea ice response in the Amundsen Sea is different from the other regions, with decreased SIE and SIV in response to the atmosphere and freshwater changes. The SIE indeed decreases by 2.7% in response to the *total* perturbation, and 37% of this decrease is induced by the freshwater perturbation. The SIV decreases by 8.1% in response to the *total* perturbation, and 40% of this decrease is induced by the freshwater perturbation. In this sector, the atmospheric perturbations dominate the SIE response over most of the year, and both the atmosphere and the freshwater perturbations play a stronger role in the summer months (Fig. 11). In early fall, the *atmosphere-induced* increase in sea-ice cover is partly inhibited by the freshwater perturbation (Fig. 11). Regarding the phase of the seasonal cycle, the freshwater perturbation advances the sea ice minimum by 6 days, while the atmosphere perturbation delays it by 9 days on average (Table 1). Unlike the two regions analyzed above, the SID in the coastal Amundsen Sea is decreased by the *total* perturbation (Fig. 12).

The *atmosphere-induced* sea ice changes in the Amundsen Sea were already described by Holland and Kwok (2012) and Holland et al. (2014) in terms of wind-driven dynamical changes (vs thermodynamical in the two previous sectors), so we focus more on the mechanisms explaining the *freshwater-induced* changes. In the coastal Amundsen Sea, the extra freshwater perturbation tends to increase the oceanic heat flux at the sea-ice base (Fig. 13-a). This result explains the modeled decrease in SIC and SIT shown in Figs. 8 and 10 respectively. Amundsen is the region of the Antarctic coast where the most rapid warming has been observed (Schmidtko et al., 2014). This is due to a number of factors that include atmospheric features, the proximity of the region to the warm Antarctic Circumpolar Current (ACC) and topographic features resulting in warm water intrusion into sub-surface waters (Walker et al., 2007; Jacobs et al., 2011; Thoma et al., 2008; Turner et al., 2017). In particular, observations have indicated intrusions of Circumpolar Deep Water (CDW) into ice-shelf cavities, with temperatures of more than 3 °C above the freezing point. This may be causing strong grounded ice-mass loss in the Antarctic basins in the sector (Shepherd et al., 2012) due to considerable ice-shelf thinning (Pritchard et al., 2012). These observations have been considered in our glacial freshwater scenario reconstruction (Section 2.2) and make the Amundsen Sea the region with the largest glacial freshwater forcing perturbation in our experimental set-up (Fig. 3).

As shown by Mathiot et al. (2017) and explained in Section 2.1, the way glacial freshwater is added into our ocean model is designed to emulate the ice-shelf cavity recirculation. It is generated by the buoyancy fluxes introduced when distributing the ice-shelf freshwater flux along the vertical of the ocean model grid points adjacent to the ice-shelf. Therefore, the inclusion of more glacial freshwater strengthens coastal overturning, which may result in a stronger heat transport from deep layers to the surface. The special conditions found in the Amundsen sector (i.e., very warm sub-surface water combined with the strongest glacial freshwater perturbation) would seem to explain the *freshwater-induced* anomaly in the oceanic heat flux reaching the ocean surface (Fig. 13-a). Indeed, as shown in Fig. 16, the extra freshwater introduced in the FW+ simulation affects the coastal stratification and promotes vertical heat transport. This leads to sub-surface cooling and surface warming in the model as also found by Jourdain et al. (2017) who explicitly modeled the ice shelf cavities of the Amundsen Sea. In the other sectors, like the Ross or Bellingshausen Seas, this feature is not dominant in our simulations compared with the impact of surface freshening on sub-surface heat convection (associated with the mechanism described in Marsland and Wolff, 2001). This warming feature of the Amundsen Sea sector is consistent with observations (Jenkins, 1999). It has been suggested that an increase in ice-shelf melting at the grounding line depth may enhance ice-shelf cavity overturning (Hellmer and Olbers, 1989) due to buoyancy changes in the

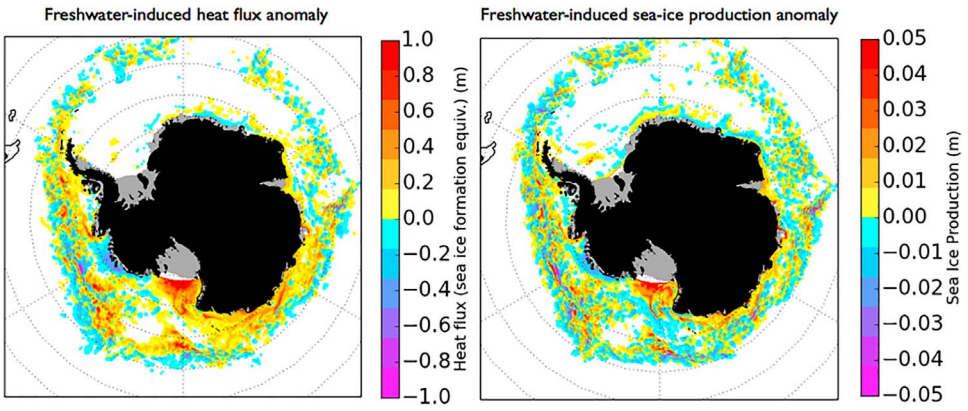

Fig. 13. Mean *freshwater-induced* changes (FW+ minus FW−) in: a) the annual mean oceanic heat flux at the sea-ice base, and b) the mean sea-ice production from March to September. Oceanic heat flux is expressed as sea-ice volume equivalent under the assumption that all the heat is used to form or melt sea-ice.

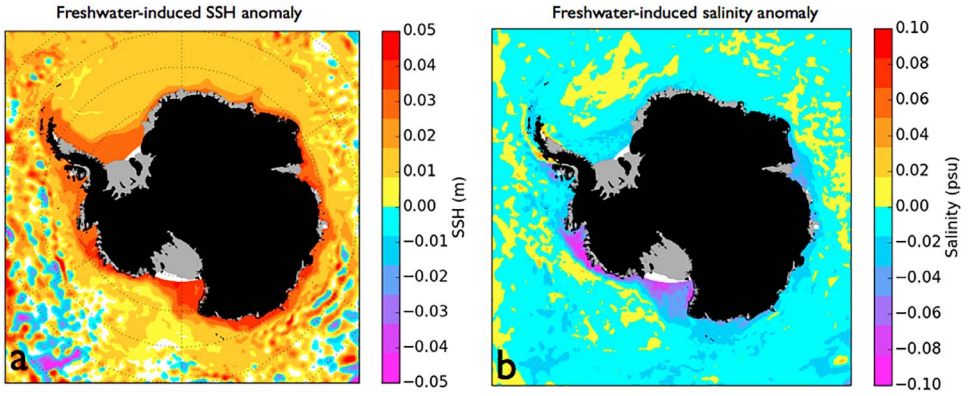

Fig. 14. Annual mean *freshwater-induced* changes (FW+ minus FW−) in: a) sea surface height (m) and b) surface salinity (psu).

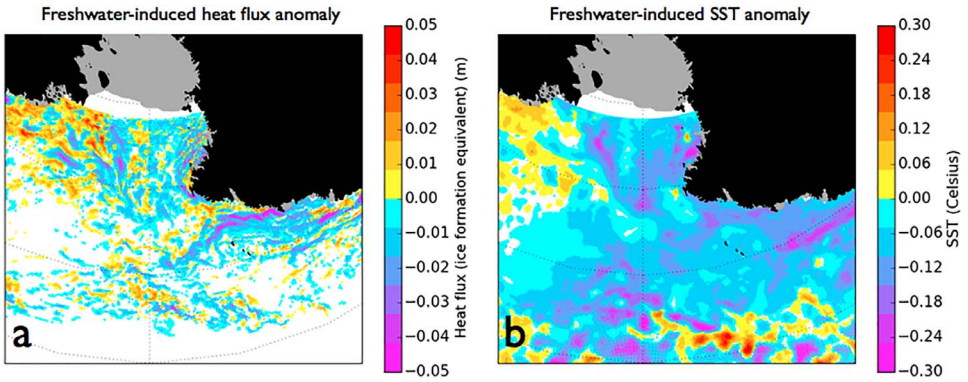

Fig. 15. December to February mean *freshwater-induced* changes (FW+ minus FW−) in: a) oceanic heat flux at the sea-ice base (expressed in sea-ice formation equivalent), and b) sea surface temperature.

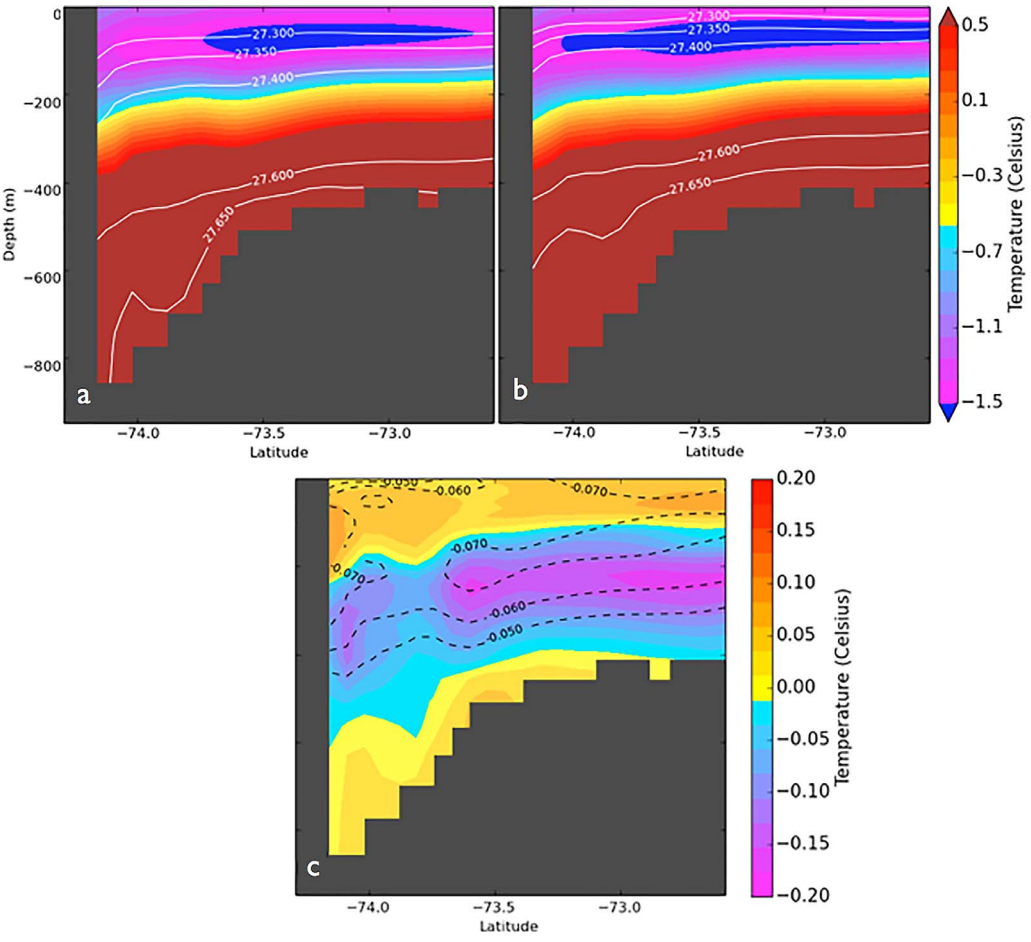

Fig. 16. Temperature and density on a vertical section perpendicular to Dotson ice shelf, Amundsen Sea (at 112.54°W), for: a) FW+, b) FW−, and c) the temperature anomalies between both simulations (FW+ minus FW−). The contours represent isodensity lines in pannels (a) and (b), and isodensity anomalies in pannel (c).

interior of the ice-shelf cavity as reproduced in our experiments. However, the magnitude of an associated heat transfer between sub-surface and surface water masses is still unclear. The inclusion of ice-shelf cavities in the ocean model should be considered, at least for this sector, in order to properly quantify the impact of ice-shelf basal melt on the very specific conditions of the Amundsen Sea sector.

5. Conclusions

The sea-ice response to recent changes in Antarctic glacial freshwater release into the Southern Ocean has been investigated with a set of eddy-permitting ocean/sea-ice/iceberg model experiments. The *freshwater-induced* changes in the global and regional sea-ice and ocean properties have been compared with typical *atmosphere-induced* changes and observations. Our model experiments consist of a control run and two perturbed simulations. The control run takes into account a recent glaciological estimate of the magnitude and spatial distribution of iceberg calving fluxes and ice-shelf basal melt fluxes. The perturbed simulations consider a decadal shift of the atmospheric variables and our own estimate of the pre-Antarctic-imbalance glacial freshwater released into the ocean. For the first time, the perturbed freshwater scenario takes into account the regional pattern of the recent ice-shelf thinning and the dynamical mass change in the grounded Antarctic basins. It is based entirely on glaciological mass budgets and represents an improvement with respect to previous studies investigating the impact of recent glacial freshwater trends on ocean properties.

Our results show that the *freshwater-induced* changes in sea-ice extent (SIE) may overall potentially contribute 25% of the *total* trend in SIE. However, the regional changes in SIE differ markedly, with freshwater accounting for 37% of the *total* decrease in SIE in the Amundsen Sea sector, but for 52% of the *total* increase in SIE in the West Pacific sector. Perturbations in freshwater forcing produce a much greater impact on sea-ice thickness, and therefore on sea-ice volume (SIV). For the entire Southern Ocean, the *freshwater-induced* changes in SIV represent almost 50% of *total* modeled changes, and are dominant with respect to the *atmosphere-induced* changes in the Ross and West Pacific sectors. In the Amundsen sector, the increased release of freshwater from the ice shelves results in an enhancement of coastal overturning as supported by regional simulations with an explicit representation of ice shelf cavities (Jourdain et al., 2017). This leads to an increase in the oceanic heat supplied by the very warm sub-surface water mass to the ocean surface near the ice sheet margin.

The *freshwater-induced* changes in SIV and SIE during the sea-ice production months are shown to have only a slight effect on the maximum of the global SIV seasonality, but with important implications for the Ice Season Duration (ISD). In the Ross and West Pacific sectors, these changes are mostly produced by *freshwater-induced* changes in the oceanic heat convection related to ocean surface freshening. Changes in the oceanic heat reaching the sea-ice base are shown to produce significant thermodynamical changes in sea-ice production. In addition, the freshening of the ocean surface results in a strengthening of the Antarctic Coastal Current (ACoC), which may induce changes in sea-ice divergence. However, such changes remain relatively weak compared with the *freshwater-induced* thermodynamical changes in sea-ice production.

Two aspects of our methodology likely lead to an underestimation of the model response to the glacial freshwater perturbation. First, the assumptions made to reconstruct the freshwater fluxes in the early 1990s are based on rates of ice sheet mass loss estimated over 1992–2011 (Section 2.2.3). Accounting for the mass loss acceleration over the most recent period would have led to a stronger difference between the two freshwater scenarios. Second, the surface salinity restoring applied to our simulations (Section 2.1) compensates a part of the perturbations in glacial freshwater fluxes. The total surface salinity restoring south of 55°S is equivalent to a freshwater flux that is 300 Gt/yr larger in FW− than in FW+. This means that over the Southern Ocean, restoring compensates 85% of the freshwater perturbation. However, a large part of this compensation occurs far from the coast once the freshwater has been advected away. For example, the freshwater flux associated with salinity restoring in the coastal Amundsen sector is only 7 Gt/yr larger in FW− than in FW+, for a perturbation in basal mass balance of 192 Gt/yr for the ice shelves of this sector. In the Ross sector, restoring is more important, accounting for a freshwater difference of 64 Gt/yr between FW− and FW+. This compensates both the extra freshwater by the ice shelves of the Ross sector (5 Gt/yr) and the advection of a significant part of the 192 Gt/yr from the Amundsen Sea (Nakayama et al., 2014). In the West Pacific/East Indian sector, surface salinity restoring compensates 34 Gt/yr of the 55 Gt/yr perturbation. In summary, surface salinity restoring unlikely affects our estimates of sea ice sensitivity in the coastal Amundsen Sea, but it probably leads to underestimate the impacts of changing glacial freshwater fluxes on sea ice properties in the Ross and West Pacific/East Indian sectors.

Most of the changes in glacial freshwater fluxes are believed to occur in the Pacific sector, especially in the Amundsen sector. In view of the strong regional contrasts in sea-ice sensitivity and associated mechanisms, we suggest that the freshwater perturbations applied to ocean models should account for these regional changes instead of uniformly spreading a perturbation around the Antarctic continent. In addition, the recently observed ice-shelf imbalance (Pritchard et al., 2012; Paolo et al., 2015) is by no means negligible compared to the imbalance of the Antarctic grounded ice sheet. Consequently, the mass loss of both the floating and the grounded parts need to be taken into account. This was not done in previous studies, which may explain a part of the differences between our results and those from similar work showing *freshwater-induced* changes in the Atlantic and East Indian sectors (Bintanja et al., 2013) or showing a very limited response of sea-ice to glacial freshwater perturbations (Pauling et al., 2016; Swart and Fyfe, 2013). There are nonetheless other differences. For example, we use an eddy-permitting resolution while the aforementioned studies used models of coarser resolution, and we use an ocean-only model (with salinity restoring) while the other studies were based on Earth System Models (no surface salinity restoring). Finally, while our wind and freshwater perturbations represent a typical decadal change from the early 1990s to the early 2000s (chosen based on available satellite data), we acknowledge that analysing a more recent period could lead to different results.

The model version, customizations, and parameters used to run the three experiments presented in this paper are provided on http://doi.org/10.5281/zenodo.1067648. The output and forcing data are available on request.

Acknowledgments

We would like to thank Jean Marc Molines for his invaluable help with model configuration. The study was partially funded by the French National Research Agency (ANR) under the SUMER (Blanc SIMI 6) 2012 project (ANR-12-BS06-0018), and the TROIS-AS project (ANR-15-CE01-0005-01). NM, JLS, GD, and NJ are part of Labex OSUG@2020 (ANR10 LABX56). NJ is an Associate Investigator of the ARC Centre of Excellence for Climate System Science. Numerical simulations were performed on IDRIS supercomputers (Saclay, France). We thank three anonymous reviewers and Editor Stephen Griffies for their useful comments and suggestions.

References

Barnier, B., Madec, G., Penduff, T., Molines, J.-M., Treguier, A.-M., Le Sommer, J., Beckmann, A., Biastoch, A., Böning, C., Dengg, J., Derval, C., Durand, E., Gulev, S., Remy, E., Talandier, C., Theetten, S., Maltrud, M., McClean, J., De Cuevas, B., 2006. Impact of partial steps and momentum advection schemes in a global ocean circulation model at eddy-permitting resolution. Ocean Dyn. 56 (5), 543–567. http://dx.doi.org/10.1007/s10236-006-0082-1.

Barrand, N., Vaughan, D., Steiner, N., Tedesco, M., Kuipers Munneke, P., Broeke, M., Hosking, J., 2013. Trends in Antarctic Peninsula surface melting conditions from observations and regional climate modeling. J. Geophys. Res. 118 (1), 315–330.
Beckmann, A., Goosse, H., 2003. A parameterization of ice shelf–ocean interaction for climate models. Ocean Model. 5 (2), 157–170.
Bell, R.E., Chu, W., Kingslake, J., Das, I., Tedesco, M., Tinto, K.J., Zappa, C.J., Frezzotti, M., Boghosian, A., Lee, W.S., 2017. Antarctic ice shelf potentially stabilized by export of meltwater in surface river. Nature 544 (7650), 344–348.
Bintanja, R., Van Oldenborgh, G., Drijfhout, S., Wouters, B., Katsman, C., 2013. Important role for ocean warming and increased ice-shelf melt in Antarctic sea-ice expansion. Nat. Geosci. 6 (5), 376–379.
Bintanja, R., Van Oldenborgh, G., Katsman, C., 2015. The effect of increased fresh water from Antarctic ice shelves on future trends in Antarctic sea ice. Ann. Glaciol. 56 (69), 120–126.
Bitz, C., Polvani, L.M., 2012. Antarctic climate response to stratospheric ozone depletion in a fine resolution ocean climate model. Geophys. Res. Lett. 39 (20).
Brodeau, L., Barnier, B., Treguier, A.-M., Penduff, T., Gulev, S., 2010. An ERA40-based atmospheric forcing for global ocean circulation models. Ocean Model. 31 (3), 88–104. https://doi.org/10.1016/j.ocemod.2009.10.005.
van den Broeke, M., 2005. Strong surface melting preceded collapse of Antarctic Peninsula ice shelf. Geophys. Res. Lett. 32 (12).
Comiso, J.C., 2010. Variability and trends of the global sea ice cover. Sea ice 2, 205–246.
Comiso, J.C., Kwok, R., Martin, S., Gordon, A.L., 2011. Variability and trends in sea ice extent and ice production in the Ross Sea. J. Geophys. Res. 116 (C4).
Cunningham, S.A., Alderson, S.G., King, B.A., Brandon, M.A., 2003. Transport and variability of the Antarctic circumpolar current in drake passage. J. Geophys. Res. Oceans 108 (C5).
Depoorter, M., Bamber, J., Griggs, J., Lenaerts, J., Ligtenberg, S., van den Broeke, M., Moholdt, G., 2013. Calving fluxes and basal melt rates of Antarctic ice-shelves. Nature 502 (7469), 89–92.
Dinniman, M.S., Klinck, J.M., Bai, L.-S., Bromwich, D.H., Hines, K.M., Holland, D.M., 2015. The effect of atmospheric forcing resolution on delivery of ocean heat to the antarctic floating ice shelves. J. Climate 28 (15), 6067–6085.
Downes, S.M., Farneti, R., Uotila, P., Griffies, S.M., Marsland, S.J., Bailey, D., Behrens, E., Bentsen, M., Bi, D., Biastoch, A., et al., 2015. An assessment of Southern Ocean water masses and sea ice during 1988–2007 in a suite of interannual CORE-II simulations. Ocean Model. 94, 67–94.
Dussin, R., Barnier, B., Brodeau, L., 2016. The making of Drakkar forcing set DFS5, DRAKKAR/MyOcean Report 01-04-16. Technical Report. LGGE, Grenoble, France. URL https://www.drakkar-ocean.eu/publications/reports/dfs5-1-report/at_download/file.
Fichefet, T., Morales Maqueda, M.A.M., 1997. Sensitivity of a global sea-ice model to the treatment of ice thermodynamics and dynamics. J. Geophys. Res. Oceans 102 (C6), 12609–12646. http://dx.doi.org/10.1029/97JC00480.
Goosse, H., Zunz, V., 2014. Decadal trends in the Antarctic sea ice extent ultimately controlled by ice–ocean feedback. Cryosphere 8 (2), 453–470.
Gouretski, V., Koltermann, K.P., 2004. WOCE global hydrographic climatology. Berichte des BSH 35, 1–52.
Griffies, S.M., Biastoch, A., Böning, C., Bryan, F., Danabasoglu, G., Chassignet, E.P., England, M.H., Gerdes, R., Haak, H., Hallberg, R.W., et al., 2009. Coordinated ocean-ice reference experiments (COREs). Ocean Model. 26 (1), 1–46.
Hellmer, H.H., Olbers, D.J., 1989. A two-dimensional model for the thermohaline circulation under an ice shelf. Antarct. Sci. 1 (04), 325–336.
Holland, P.R., Bruneau, N., Enright, C., Losch, M., Kurtz, N.T., Kwok, R., 2014. Modeled trends in Antarctic sea ice thickness. J. Climate 27 (10), 3784–3801.
Holland, P.R., Kwok, R., 2012. Wind-driven trends in Antarctic sea-ice drift. Nat. Geosci. 5 (12), 872–875. http://dx.doi.org/10.1038/ngeo1627.
Hughes, T.J., 1981. The weak underbelly of the West Antarctic ice-Sheet. Earth Sci. Faculty Schol. 156. URL http://digitalcommons.library.umaine.edu/ers_facpub/156.
Irvine-Fynn, T.D., Hodson, A.J., Moorman, B.J., Vatne, G., Hubbard, A.L., 2011. Polythermal glacier hydrology: a review. Rev. Geophys. 49 (4).
Jacobs, S., Giulivi, C., Mele, P., 2002. Freshening of the Ross Sea during the late 20th century. Science 297 (5580), 386–389.
Jacobs, S.S., Giulivi, C.F., 2010. Large multidecadal salinity trends near the Pacific–Antarctic continental margin. J. Climate 23 (17), 4508–4524.
Jacobs, S.S., Jenkins, A., Giulivi, C.F., Dutrieux, P., 2011. Stronger ocean circulation and increased melting under Pine Island Glacier ice shelf. Nat. Geosci. 4 (8), 519–523.
Jenkins, A., 1999. The impact of melting ice on ocean waters. J. Phys. Oceanogr. 29 (9), 2370–2381.
Jourdain, N.C., Mathiot, P., Merino, N., Durand, G., Le Sommer, J., Spence, P., Dutrieux, P., Madec, G., 2017. Ocean circulation and sea-ice thinning induced by melting ice shelves in the Amundsen Sea. J. Geophys. Res. 122 (3), 2550–2573.
Kwok, R., Comiso, J.C., Lee, T., Holland, P.R., 2016. Linked trends in the South Pacific sea ice edge and Southern Oscillation Index. Geophys. Res. Lett. 43 (19).
Lefebvre, W., Goosse, H., 2008. An analysis of the atmospheric processes driving the large-scale winter sea ice variability in the Southern Ocean. J. Geophys. Res. 113 (C2).
Lenaerts, J., Den Broeke, M., Berg, W., Meijgaard, E.v., Kuipers Munneke, P., 2012. A new, high-resolution surface mass balance map of Antarctica (1979–2010) based on regional atmospheric climate modeling. Geophys. Res. Lett. 39 (4).
Liu, Y., Moore, J.C., Cheng, X., Gladstone, R.M., Bassis, J.N., Liu, H., Wen, J., Hui, F., 2015. Ocean-driven thinning enhances iceberg calving and retreat of Antarctic ice shelves. Proc. Natl. Acad. Sci. U.S.A 112 (11), 3263–3268.
Madec, G., 2014. NEMO Ocean Engine, Institut Pierre-Simon Laplace (IPSL). Note du Pȳle de modĘlisation.
Mantyla, A.W., Reid, J.L., 1983. Abyssal characteristics of the World Ocean waters. Deep-Sea Res. 30 (8), 805–833.
Marsh, R., Ivchenko, V.O., Skliris, N., Alderson, S., Bigg, G.R., Madec, G., Blaker, A.T., Aksenov, Y., Sinha, B., Coward, A.C., Le Sommer, J., Merino, N., Zalesny, V.B., 2015. NEMO-ICB (v1.0): interactive icebergs in the NEMO ocean model globally configured at eddy-permitting resolution. Geosci. Model Dev. 8 (5), 1547–1562. http://dx.doi.org/10.5194/gmd-8-1547-2015.
Marsland, S., Wolff, J.-O., 2001. On the sensitivity of southern ocean sea-ice to the surface freshwater flux: a model study. J. Geophys. Res. Oceans 106 (C2), 2723–2741.
Mathiot, P., Jenkins, A., Harris, C., Madec, G., 2017. Explicit representation and parametrised impacts of under ice shelf seas in the zcoordinate ocean model NEMO 3.6. Geosci. Model Dev. 10 (7), 2849.
Merino, N., Le Sommer, J., Durand, G., Jourdain, N.C., Madec, G., Mathiot, P., Tournadre, J., 2016. Antarctic icebergs melt over the Southern Ocean: climatology and impact on sea ice. Ocean Model. 104, 99–110.
Monaghan, A.J., Bromwich, D.H., Fogt, R.L., Wang, S.-H., Mayewski, P.A., Dixon, D.A., Ekaykin, A., Frezzotti, M., Goodwin, I., Isaksson, E., et al., 2006. Insignificant change in Antarctic snowfall since the International Geophysical Year. Science 313 (5788), 827–831.
Nakayama, Y., Timmermann, R., Rodehacke, C.B., Schröder, M., Hellmer, H.H., 2014. Modeling the spreading of glacial meltwater from the Amundsen and Bellingshausen Seas. Geophys. Res. Lett. 41 (22), 7942–7949.
Nicolas, J.P., Vogelmann, A.M., Scott, R.C., Wilson, A.B., Cadeddu, M.P., Bromwich, D.H., Verlinde, J., Lubin, D., Russell, L.M., Jenkinson, C., et al., 2017. January 2016 extensive summer melt in West Antarctica favoured by strong El Niño. Nat. Commun. 8.
Orsi, A., Johnson, G., Bullister, J., 1999. Circulation, mixing, and production of Antarctic Bottom Water. Prog. Oceanogr. 43 (1), 55–109.
Paolo, F.S., Fricker, H.A., Padman, L., 2015. Volume loss from Antarctic ice shelves is accelerating. Science 348 (6232), 327–331.
Pauling, A.G., Bitz, C.M., Smith, I.J., Langhorne, P.J., 2016. The response of the Southern Ocean and Antarctic Sea ice to fresh water from ice shelves in an earth system model. J. Climate 29 (5), 1655–1672.
Pauling, A.G., Smith, I.J., Langhorne, P.J., Bitz, C.M., 2017. Time-dependent freshwater input from ice shelves: impacts on Antarctic sea ice and the southern ocean in an earth system model. Geophys. Res. Lett. 44 (20), 10454–10461.
Perovich, D.K., 2011. The changing arctic sea ice cover. Oceanography 24 (3), 162–173.
Polvani, L.M., Smith, K.L., 2013. Can natural variability explain observed Antarctic sea ice trends? New modeling evidence from CMIP5. Geophys. Res. Lett. 40 (12), 3195–3199.
Pritchard, H., Ligtenberg, S., Fricker, H., Vaughan, D., Van den Broeke, M., Padman, L., 2012. Antarctic ice-sheet loss driven by basal melting of ice shelves. Nature 484 (7395), 502–505.
Rignot, E., Bamber, J.L., Van Den Broeke, M.R., Davis, C., Li, Y., Van De Berg, W.J., Van Meijgaard, E., 2008. Recent Antarctic ice mass loss from radar interferometry and regional climate modelling. Nat. Geosci. 1 (2), 106–110.
Rignot, E., Jacobs, S., Mouginot, J., Scheuchl, B., 2013. Ice-shelf melting around Antarctica. Science 341 (6143), 266–270.
Rignot, E., Vaughan, D.G., Schmeltz, M., Dupont, T., MacAyeal, D., 2002. Acceleration of Pine island and Thwaites glaciers, west Antarctica. Ann. Glaciol. 34 (1), 189–194.
Rignot, E., Velicogna, I., van den Broeke, M.R., Monaghan, A., Lenaerts, J.T., 2011. Acceleration of the contribution of the Greenland and Antarctic ice sheets to sea level rise. Geophys. Res. Lett. 38 (5).
Roemmich, D., Church, J., Gilson, J., Monselesan, D., Sutton, P., Wijffels, S., 2015. Unabated planetary warming and its ocean structure since 2006. Nat. Clim. Change 5 (3), 240–245.
Rott, H., Skvarca, P., Nagler, T., 1996. Rapid collapse of northern Larsen ice shelf, Antarctica. Science 271 (5250), 788.
Rye, C.D., Garabato, A.C.N., Holland, P.R., Meredith, M.P., Nurser, A.G., Hughes, C.W., Coward, A.C., Webb, D.J., 2014. Rapid sea-level rise along the Antarctic margins in response to increased glacial discharge. Nat. Geosci. 7 (10), 732–735.
Sallée, J.-B., Matear, R.J., Rintoul, S.R., Lenton, A., 2012. Localized subduction of anthropogenic carbon dioxide in the Southern Hemisphere oceans. Nat. Geosci. 5 (8), 579–584.
Scambos, T.A., Bohlander, J., Shuman, C.u., Skvarca, P., 2004. Glacier acceleration and thinning after ice shelf collapse in the Larsen B embayment, Antarctica. Geophys. Res. Lett. 31 (18).
Schmidtko, S., Heywood, K.J., Thompson, A.F., Aoki, S., 2014. Multidecadal warming of Antarctic waters. Science 346 (6214), 1227–1231.
Screen, J.A., 2011. Sudden increase in Antarctic sea ice: fact or artifact? Geophys. Res. Lett. 38 (13).
Shepherd, A., Ivins, E.R., Geruo, A., Barletta, V.R., Bentley, M.J., Bettadpur, S., Briggs, K.H., Bromwich, D.H., Forsberg, R., Galin, N., et al., 2012. A reconciled estimate of ice-sheet mass balance. Science 338 (6111), 1183–1189.
Sigmond, M., Fyfe, J., 2010. Has the ozone hole contributed to increased Antarctic sea ice extent? Geophys. Res. Lett. 37 (18).
Smith, J., Andersen, T., Shortt, M., Gaffney, A., Truffer, M., Stanton, T., Bindschadler, R., Dutrieux, P., Jenkins, A., Hillenbrand, C.-D., et al., 2016. Sub-ice-shelf sediments record history of twentieth-century retreat of Pine Island Glacier. Nature 541 (7635), 77–80.
Stammerjohn, S., Martinson, D., Smith, R., Yuan, X., Rind, D., 2008. Trends in Antarctic annual sea ice retreat and advance and their relation to el niño–Southern oscillation and southern annular mode variability. J. Geophys. Res. Oceans 113 (C3).
Stammerjohn, S., Massom, R., Rind, D., Martinson, D., 2012. Regions of rapid sea ice change: an inter-hemispheric seasonal comparison. Geophys. Res. Lett. 39 (6).
Steele, M., Morley, R., Ermold, W., 2001. PHC: a global ocean hydrography with a high-quality Arctic Ocean. J. Climate 14 (9), 2079–2087.
Sutterley, T.C., Velicogna, I., Rignot, E., Mouginot, J., Flament, T., Van Den Broeke, M.R.,

Van Wessem, J.M., Reijmer, C.H., 2014. Mass loss of the Amundsen Sea Embayment of West Antarctica from four independent techniques. Geophys. Res. Lett. 41 (23), 8421–8428.
Swart, N., Fyfe, J., 2013. The influence of recent Antarctic ice sheet retreat on simulated sea ice area trends. Geophys. Res. Lett. 40 (16), 4328–4332.
Thoma, M., Jenkins, A., Holland, D., Jacobs, S., 2008. Modelling circumpolar deep water intrusions on the Amundsen Sea continental shelf, Antarctica. Geophys. Res. Lett. 35 (18).
Thompson, D.W., Solomon, S., Kushner, P.J., England, M.H., Grise, K.M., Karoly, D.J., 2011. Signatures of the Antarctic ozone hole in Southern Hemisphere surface climate change. Nat. Geosci. 4 (11), 741–749.
Tréguier, A.-M., Le Sommer, J., Molines, J.-M., De Cuevas, B., 2010. Response of the Southern Ocean to the Southern annular mode: interannual variability and multi-decadal trend. J. Phys. Oceanogr. 40 (7), 1659–1668.
Turner, J., Bracegirdle, T.J., Phillips, T., Marshall, G.J., Hosking, J.S., 2013. An initial assessment of Antarctic sea ice extent in the CMIP5 models. J. Climate 26 (5), 1473–1484.
Turner, J., Comiso, J.C., Marshall, G.J., Lachlan-Cope, T.A., Bracegirdle, T., Maksym, T., Meredith, M.P., Wang, Z., Orr, A., 2009. Non-annular atmospheric circulation change induced by stratospheric ozone depletion and its role in the recent increase of Antarctic sea ice extent. Geophys. Res. Lett. 36 (8).
Turner, J., Orr, A., Gudmundsson, G.H., Jenkins, A., Bingham, R.G., Hillenbrand, C.-D., Bracegirdle, T.J., 2017. Atmosphere-ocean-ice interactions in the Amundsen Sea Embayment, West Antarctica. Rev. Geophys. 55 (1), 235–276.
Walker, D.P., Brandon, M.A., Jenkins, A., Allen, J.T., Dowdeswell, J.A., Evans, J., 2007. Oceanic heat transport onto the Amundsen Sea shelf through a submarine glacial trough. Geophys. Res. Lett. 34 (2).
Zhang, J., 2007. Increasing Antarctic sea ice under warming atmospheric and oceanic conditions. J. Climate 20 (11), 2515–2529.